The solution of the hypernetted chain and Percus–Yevick approximations for fluids of hard nonspherical particles. Results for hard ellipsoids of revolution

A. Perera, P. G. Kusalik, and G. N. Patey
Department of Chemistry, University of British Columbia, Vancouver, British Columbia V6T 1Y6, Canada

(Received 20 January 1987; accepted 13 March 1987)

In this paper we describe a general approach which allows the hypernetted chain (HNC) and Percus–Yevick (PY) integral equation theories to be solved numerically for fluids of *hard* nonspherical particles. Explicit results are given for fluids of hard ellipsoids of revolution and comparisons are made with recent Monte Carlo calculations. It is found that for dense systems of highly anisotropic ellipsoids the HNC and PY closures give significantly different results. The HNC theory is superior predicting the existance of a nematic phase in qualitative agreement with computer simulations. The PY approximation strongly and erroneously suggests that the isotropic phase is stable throughout the liquid regime.

I. INTRODUCTION

The purpose of this paper is to describe a method which allows the hypernetted chain (HNC) and Percus–Yevick (PY) integral equation theories to be solved for fluids of hard nonspherical particles and to give explicit results for hard ellipsoids of revolution. The present approach closely follows that described in earlier papers,[1–5] but some extension of the theory is necessary in order to account for the fact that pair potentials which characterize the interaction of *hard* nonspherical objects are discontinuous in orientational space. The method given here allows the integral equation theories to be solved for hard particles of arbitrary shape provided that the minimum contact distance between two particles is a known function of the particle orientations. For example, this contact function is known for ellipsoids,[6,7] spherocylinders,[8] and for particles of any shape which can be represented by aggregates of fused hard spheres.

This paper also includes a detailed analysis of the HNC and PY theories for fluids consisting of hard ellipsoids of revolution. Fluids of ellipsoids with length-to-breadth ratios $a/b = 1.25, 2, 3$, and 5 are studied for different densities, and insofar as possible, comparisons are made with the extensive Monte Carlo (MC) calculations of Frenkel and Mulder[9] and with those of Perram *et al.*[10] We also investigate the stability limits of the isotropic phase with respect to fluctuations of nematic symmetry. This is done using the stability conditions put forward by Stecki and Kloczkowski[11] as discussed in our earlier paper[5] dealing with simple liquid crystal models. Indeed, it is in this regard that one finds an interesting difference between the HNC and PY approximations. If a/b is sufficiently large the HNC theory shows an orientational instability at liquid densities. Furthermore, for $a/b = 3$ the system becomes orientationally unstable at a density which is in good agreement with the isotropic–nematic transition observed by Frenkel and Mulder.[9] This is not true for the PY approximation which does not predict an orientational instability at densities lower than the Monte Carlo freezing transition.[9] Thus the tendency of ellipsoids to align and form a nematic phase if $a/b \gtrsim 2.75$ (cf. Ref. 9) is not well described by the PY theory. The equations of state and the pair correlation functions given by the HNC and PY theories are also compared and evaluated in the text.

The remainder of this paper is divided into three parts. The method of solution is discussed in Sec. II, results for ellipsoids are given in Sec. III, and our conclusions are summarized in Sec. IV.

II. THEORY

In this section we consider hard nonspherical objects of arbitrary shape. For particles of this type the pair potential $u(\mathbf{r},\Omega_1,\Omega_2)$ can be expressed in the form

$$u(\mathbf{r},\Omega_1,\Omega_2) = \begin{cases} \infty, & \text{if particles 1 and 2 overlap} \\ 0, & \text{if particles 1 and 2 do not overlap} \end{cases}, \tag{1}$$

where Ω_1 and Ω_2 represent Euler angles describing the orientations of particles 1 and 2 and $\mathbf{r}$ is the vector joining the centers of mass.

A. The HNC and PY theories

If $h(\mathbf{r},\Omega_1,\Omega_2)$ and $c(\mathbf{r},\Omega_1,\Omega_2)$ are the pair and direct correlation functions, respectively, and if we let $\eta(12) = h(12) - c(12)$, then the HNC and PY integral equation theories are given by the Ornstein–Zernike (OZ) equation

$$\eta(12) = \frac{\rho}{8\pi^2}\int c(13)[\eta(32) + c(32)]d(3)\,, \tag{2}$$

coupled with the closure relationships

$$c(12) = -1 - \eta(12) \quad \text{overlap}\,, \tag{3a}$$

$$c(12) = c_{\mathrm{CL}}(12) \quad \text{no overlap}\,, \tag{3b}$$

where ρ is the number density, $d(3) = d\Omega_3\, d\mathbf{r}_3$, and $c_{\mathrm{CL}}(12)$ represents either the HNC or the PY approximation. In general the HNC and PY closures are given by[12]

$$c_{\mathrm{HNC}}(12) = h(12) - \ln g(12) - \beta u(12) \tag{4a}$$

and

$$c_{\mathrm{PY}}(12) = g(12)[e^{-\beta u(12)} - 1]\,, \tag{4b}$$

 0021-9606/87/141295-12$02.10

where $g(12) = h(12) + 1$ and $\beta = 1/kT$. For hard nonspherical particles it is clear that these equations become

$$c_{\mathrm{HNC}}(12) = h(12) - \ln g(12) \tag{5a}$$

and

$$c_{\mathrm{PY}}(12) = 0 \tag{5b}$$

if the particles *do not overlap*.

The reduction and solution of Eqs. (2) and (3) with $c_{\mathrm{CL}}(12)$ given by Eqs. (5a) or (5b) closely follows the approach employed in previous papers.[1,2] Therefore, here we given only a brief summary of the basic results and a discussion of the extensions necessary in order to deal with fluids of hard nonspherical particles. For a more complete description of the method the reader is referred to Refs. 1 and 2.

In order to reduce and solve Eqs. (2) and (3) it is necessary to expand all correlation functions in the form[1,2,13,14]

$$F(12) = \sum_{\substack{mnl \\ \mu\nu}} F^{mnl}_{\mu\nu}(r)\Phi^{mnl}_{\mu\nu}(\Omega_1,\Omega_2,\hat{\mathbf{r}}) , \tag{6a}$$

where the coefficients $F^{mnl}_{\mu\nu}(r)$ are defined by

$$F^{mnl}_{\mu\nu}(r) = \frac{1}{I^{mnl}_{\mu\nu}} \int F(12)\Phi^{mnl*}_{\mu\nu}(12)d\Omega_1\, d\Omega_2 , \tag{6b}$$

$$I^{mnl}_{\mu\nu} = \int \Phi^{mnl}_{\mu\nu}(12)\Phi^{mnl*}_{\mu\nu}(12)\, d\Omega_1\, d\Omega_2 . \tag{6c}$$

As in earlier work[1,2] the rotational invariants $\Phi^{mnl}_{\mu\nu}(12)$ are defined by

$$\Phi^{mnl}_{\mu\nu}(12) = f^{mnl} \sum_{\mu'\nu'\lambda'} \begin{pmatrix} m & n & l \\ \mu' & \nu' & \lambda' \end{pmatrix} \times R^{\,m}_{\mu'\mu}(\Omega_1) R^{\,n}_{\nu'\nu}(\Omega_2) R^{\,l}_{\lambda' 0}(\hat{\mathbf{r}}) , \tag{6d}$$

where $\hat{\mathbf{r}} = (\mathbf{r}_2 - \mathbf{r}_1)/|\mathbf{r}_2 - \mathbf{r}_1|$, $R^{\,m}_{\mu'\mu}(\Omega_1)$ is a Wigner generalized spherical harmonic[15] and f^{mnl} can be any nonzero constant. It is useful to note that the rotational invariants satisfy the orthogonality condition[14,16]:

$$\frac{1}{(8\pi^2)^2} \int \Phi^{m'n'l'}_{\mu'\nu'}(12)\Phi^{mnl*}_{\mu\nu}(12)d\Omega_1\, d\Omega_2 = \frac{(f^{mnl})^2}{(2m+1)(2n+1)(2l+1)} \delta^{mnl\mu\nu}_{m'n'l'\mu'\nu'} , \tag{7a}$$

where

$$\delta^{mnl\mu\nu}_{m'n'l'\mu'\nu'} = \delta_{mm'}\delta_{nn'}\delta_{ll'}\delta_{\mu\mu'}\delta_{\nu\nu'} . \tag{7b}$$

In Fourier space the correlation function expansions allow the OZ equation to be reduced[13,1] to a set of algebraic equations relating the Hankel transforms $\tilde{\eta}^{mnl}_{\mu\nu}(k)$ and $\tilde{c}^{mnl}_{\mu\nu}(k)$ defined by the general expression

$$\tilde{F}^{mnl}_{\mu\nu}(k) = 4\pi i^l \int_0^\infty r^2 j_l(kr) F^{mnl}_{\mu\nu}(r)dr , \tag{8a}$$

where $j_l(kr)$ is a spherical Bessel function. For reference below, it is useful to note here that if $F^{mnl}_{\mu\nu}(r)$ decays more rapidly than $1/r^3$ as $r \to \infty$, then

$$\tilde{F}^{mnl}_{\mu\nu}(k=0) = 0, \quad \text{for all } l \neq 0 . \tag{8b}$$

It is also possible[1,2,7] to expand (essentially analytically) the HNC and PY closures in the same basis set of rotational invariants. For potentials which are continuous functions of the orientational variables this allows the HNC and PY equations to be solved as described in Refs. 1 and 2, respectively. However, for the hard nonspherical models considered in the present paper the problem is complicated by the fact that $c(\mathbf{r},\Omega_1,\Omega_2)$ and $h(\mathbf{r},\Omega_1,\Omega_2)$ are discontinuous functions of Ω_1 and Ω_2 as well as of $\mathbf{r}$. In the numerical solution of the integral equation theories, the discontinuous behavior must be taken into account as described below.

From the definition (6b) we have the relationship

$$I^{mnl}_{\mu\nu} c^{mnl}_{\mu\nu}(r) = \int c(12)\Phi^{mnl*}_{\mu\nu}(12)d\Omega_1\, d\Omega_2 , \tag{9}$$

where $I^{mnl}_{\mu\nu}$ is given by Eq. (6c). For fixed r, we can split the integral in Eq. (9) into two parts corresponding to the regions of orientational space where the particles *do* and *do not* overlap. Thus we have

$$I^{mnl}_{\mu\nu} c^{mnl}_{\mu\nu}(r) = \int_{\mathrm{OV}} c(12)\Phi^{mnl*}_{\mu\nu}(12)d\Omega_1\, d\Omega_2 + \int_{\mathrm{NOV}} c(12)\Phi^{mnl*}_{\mu\nu}(12)d\Omega_1\, d\Omega_2 , \tag{10}$$

where OV denotes the *overlap* and NOV in the *nonoverlap* regions. Applying the closure relations (3a) and (3b), Eq. (10) becomes

$$I^{mnl}_{\mu\nu} c^{mnl}_{\mu\nu}(r) = \int_{\mathrm{OV}} [-1 - \eta(12)]\Phi^{mnl*}_{\mu\nu}(12)d\Omega_1\, d\Omega_2 + \int_{\mathrm{NOV}} c_{\mathrm{CL}}(12)\Phi^{mnl*}_{\mu\nu}(12)d\Omega_1\, d\Omega_2 . \tag{11}$$

If $\eta(12)$ and $c_{\mathrm{CL}}(12)$ are now expanded in rotational invariants we obtain

$$c^{mnl}_{\mu\nu}(r) = \sum_{\substack{m'n'l' \\ \mu'\nu'}} [-\delta^{m'n'l'\mu'\nu'}_{00000} - \eta^{m'n'l'}_{\mu'\nu'}(r)] A^{\,mnl\mu\nu}_{m'n'l'\mu'\nu'}(r) + \sum_{\substack{m'n'l' \\ \mu'\nu'}} c^{m'n'l'}_{\mathrm{CL};\mu'\nu'}(r)\, B^{\,mnl\mu\nu}_{m'n'l'\mu'\nu'}(r) , \tag{12a}$$

where

$$A^{\,mnl\mu\nu}_{m'n'l'\mu'\nu'}(r) = \frac{1}{I^{mnl}_{\mu\nu}} \int_{\mathrm{OV}} \Phi^{mnl*}_{\mu\nu}(12)\Phi^{m'n'l'}_{\mu'\nu'}(12)d\Omega_1\, d\Omega_2 , \tag{12b}$$

$$B^{\,mnl\mu\nu}_{m'n'l'\mu'\nu'}(r) = \frac{1}{I^{mnl}_{\mu\nu}} \int_{\mathrm{NOV}} \Phi^{mnl*}_{\mu\nu}(12)\Phi^{m'n'l'}_{\mu'\nu'}(12)d\Omega_1\, d\Omega_2 . \tag{12c}$$

It is also clear from the orthogonality condition (7a) that the simple relationship

$$B^{\,mnl\mu\nu}_{m'n'l'\mu'\nu'}(r) = \delta^{mnl\mu\nu}_{m'n'l'\mu'\nu'} - A^{\,mnl\mu\nu}_{m'n'l'\mu'\nu'}(r) , \tag{13}$$

must hold. Equation (13) allows Eq. (12a) to be expressed in the final convenient form

$$c^{mnl}_{\mu\nu}(r) = \sum_{\substack{m'n'l' \\ \mu'\nu'}} [-\delta^{m'n'l'\mu'\nu'}_{00000} - \eta^{m'n'l'}_{\mu'\nu'}(r) - c^{m'n'l'}_{\mathrm{CL};\mu'\nu'}(r)] \times A^{\,mnl\mu\nu}_{m'n'l'\mu'\nu'}(r) + c^{mnl}_{\mathrm{CL};\mu\nu}(r) , \tag{14}$$

which is valid for all values of r.

There are several points worthy of note. If we let a and b be distances such that if $r<b$ the particles overlap for all orientations, and if $r>a$ the particles do not overlap for any orientation, then it is evident that for $r<b$,

$$A^{mnl\mu\nu}_{m'n'l'\mu'\nu'}(r)=\delta^{mnl\mu\nu}_{m'n'l'\mu'\nu'}\,, \tag{15a}$$

$$c^{mnl}_{\mu\nu}(r)=-\delta^{mnl\mu\nu}_{00000}-\eta^{mnl}_{\mu\nu}(r)\,, \tag{15b}$$

and for $r>a$,

$$A^{mnl\mu\nu}_{m'n'l'\mu'\nu'}(r)=0\,, \tag{16a}$$

$$c^{mnl}_{\mu\nu}(r)=c^{mnl}_{\mathrm{CL};\mu\nu}(r)\,. \tag{16b}$$

Thus both terms in Eq. (14) only apply in the intermediate region where $b<r<a$. It is also clear that the $A^{mnl\mu\nu}_{m'n'l'\mu'\nu'}(r)$ and consequently the projections $c^{mnl}_{\mu\nu}(r)$ must be continuous functions of r for hard *nonspherical* particles. This differs from models previously studied[1,2,4] (i.e., multipolar hard spheres) where the hard *spherical* core introduces discontinuities in the $c^{mnl}_{\mu\nu}(r)$ coefficients at the hard sphere diameter. Finally, we remark that Eq. (14) is not restricted to simple hard objects but could also be used to solve the HNC and PY theories for decorated hard nonspherical particles such as multipolar ellipsoids.

In actual applications the $c^{mnl}_{\mathrm{CL};\mu\nu}$ (CL≡HNC or PY) projections used in Eq. (14) are obtained from the HNC or PY expansions given in Refs. 1 and 2, respectively. For simple hard objects these give

$$c^{mnl}_{\mathrm{PY};\mu\nu}(r)=0 \tag{17}$$

and

$$c^{mnl}_{\mathrm{HNC};\mu\nu}(r)=\sum_{\substack{m_1n_1l_1\\ \mu_1\nu_1}}\sum_{\substack{m_2n_2l_2\\ \mu_2\nu_2}}p\int_r^\infty h^{m_1n_1l_1}_{\mu_1\nu_1}(r')\times\frac{\partial}{\partial r'}\left[-\eta^{m_2n_2l_2}_{\mu_2\nu_2}(r')\right]dr'\,, \tag{18}$$

where p depends upon all 15 indicies and its definition is apparent from Eqs. (23) of Ref. 1. Also we note that the $A^{mnl\mu\nu}_{m'n'l'\mu'\nu'}(r)$ functions must in general be found by numerical integration of Eq. (12b).

B. The equation of state

The equation of state can be obtained from the virial or from the compressibility equations. Of course, in an exact calculation both routes must give the same result, but this is not true for approximate theories such as the HNC and PY approximations.[12]

In general for isotropic fluids the virial equation of state can be expressed in the form

$$\frac{\beta P}{\rho}=1-\frac{2\pi}{3}\beta\rho\frac{1}{(8\pi^2)^2}\times\int d\Omega_1\,d\Omega_2\int dr\,r^3\frac{\partial u(r,\Omega_1,\Omega_2)}{\partial r}g(r,\Omega_1,\Omega_2)\,, \tag{19}$$

where P is the pressure. If $u(r,\Omega_1,\Omega_2)$ is given by Eq. (1), then for fixed Ω_1 and Ω_2 (now expressed in an intermolecular coordinate system) integration over r can be carried out[12] to give

$$\frac{\beta P}{\rho}=1+\frac{2\pi}{3}\rho\frac{1}{(8\pi^2)^2}\int d\Omega_1\,\Omega_2\sigma(\Omega_1,\Omega_2)^3g(\sigma,\Omega_1,\Omega_2)\,, \tag{20}$$

where $\sigma(\Omega_1,\Omega_2)$ is the contact distance for fixed orientations Ω_1 and Ω_2. Expanding $g(12)$ in rotational invariants immediately yield

$$\frac{\beta P}{\rho}=1+\frac{2\pi\rho}{3}\frac{1}{(8\pi^2)^2}\times\sum_{\substack{mnl\\ \mu\nu}}\int d\Omega_1\,d\Omega_2\sigma(12)^3g^{mnl}_{\mu\nu}(\sigma)\Phi^{mnl}_{\mu\nu}(12)\,. \tag{21}$$

Thus the virial expression for the compressibility factor depends upon all terms in the rotational invariant expansion of $g(12)$.

If $\sigma(\Omega_1,\Omega_2)$ and $g(\sigma,\Omega_1,\Omega_2)$ are known, then Eq. (20) can be integrated numerically to give the equation of state. However, a word of caution is in order. In general in numerical calculations the value of σ for given Ω_1 and Ω_2 will not exactly coincide with an r-space grid point. Therefore, in order to obtain a value for $g(\sigma,\Omega_1,\Omega_2)$ an extrapolation is required. Now, since $g(r,\Omega_1,\Omega_2)$ is discontinuous at $r=\sigma$ and varies rapidly in this region, numerical extrapolations are usually not very accurate. Therefore, in HNC and PY calculations a much better method is to first determine $\eta(\sigma,\Omega_1,\Omega_2)$ by interpolation of the continuous function $\eta(r,\Omega_1,\Omega_2)$. The required values of $g(\sigma,\Omega_1,\Omega)$ are then given by the relationships

$$g(\sigma,\Omega_1,\Omega_2)=e^{\eta(\sigma,\Omega_1,\Omega_2)};\quad \mathrm{HNC}\,, \tag{22a}$$

and

$$g(\sigma,\Omega_1,\Omega_2)=1+\eta(\sigma,\Omega_1,\Omega_2);\quad \mathrm{PY}\,, \tag{22b}$$

which can be easily deduced from Eqs. (1) and (4).

The equation of state can also be obtained from the compressibility equation which can be expressed in the form[12]

$$\beta\left(\frac{\partial P}{\partial\rho}\right)_T=\frac{\chi^0_T}{\chi_T}=\frac{1}{[1+\rho\tilde{h}^{000}_{00}(k=0)]}\,, \tag{23}$$

where χ_T is the isothermal compressibility and $\chi^0_T=\beta/\rho$ is the ideal gas result. In Appendix A the OZ equation together with Eq. (8a) is used to show that the relationship

$$1+\rho\tilde{h}^{000}_{00}(k=0)=\frac{1}{[1-\rho\tilde{c}^{000}_{00}(k=0)]}\,, \tag{24}$$

which is very useful in the theory of spherical particles,[12] also holds in the hard nonspherical case. Therefore, Eq. (23) can also be written as

$$\beta\left(\frac{\partial P}{\partial\rho}\right)_T=1-\rho\tilde{c}^{000}_{00}\,(k=0)\,. \tag{25}$$

Finally, the compressibility factor, $\beta P/\rho$ can be determined by numerical integration of the equation

$$\frac{\beta P}{\rho}=1+\frac{1}{\rho}\int_0^\rho\left[\beta\left(\frac{\partial P}{\partial\rho'}\right)_T\right]d\rho'\,. \tag{26}$$

III. HARD ELLIPSOIDS OF REVOLUTIONS

We consider hard ellipsoids of revolution characterized by the length-to-breadth ratio a/b. In the present work it is

TABLE I. The terms included in the different basis sets. In all cases $m_{max} = n_{max}$ and $l_{max} < 6$.

Basis set	No. of independent terms (N_i)	No. of independent $A^{mnl}_{m'n'l'}(r)$ coefficients[b]	Terms included[a]
I			
			(000),(022),(220),(222)
			(224),(044),(242),(244)
			(246),(440),(442),(444)
($m_{max} = 4$)	13	106	(446)
II			
			(066),(264),(266),(462)
			(464),(466),(660),(662)
($m_{max} = 6$)	23	342	(664),(666)
III			
			(286),(484),(486),(682)
			(684),(686),(880),(882)
($m_{max} = 8$)	33	714	(884),(886)

[a] Here we list only the additional terms which occur in each basis set. The total set is the sum of the additional plus all previous terms.

[b] The total number of $A^{mnl}_{m'n'l'}(r)$ coefficients is $N_A = [N_i(N_i + 1)/2] + [N_{ni}(N_{ni} + 1)/2]$, where N_i is the number of independent terms and N_{ni} is the number of pairs of terms related by Eq. (27).

convenient to define a state of the ellipsoidal fluid by specifying the reduced density $\rho^* = \rho b^3$. All numerical calculations were carried out using 1024 grid points and the grid width Δr was $0.01b$ for $a/b < 3$ and $0.02b$ for $a/b = 5$. Percus–Yevick and HNC results are given for $a/b = 1.25$, 2, 3, and 5, and for the first three cases comparisons are made with the Monte Carlo calculations of Frenkel and Mulder.[19] Computer simulation results are not available for values of a/b larger than 3.

Ellipsoids of revolution have axial symmetry together with a center of inversion. This means that only terms for which $\mu = \nu = 0$ and m, n, and l are even, are allowed in the correlation function expansions. Furthermore, the expansion coefficients must satisfy the relationship

$$F^{mnl}_{00}(r) = F^{nml}_{00}(r) , \tag{27}$$

where $F \equiv h$, c, or η. These symmetry requirements will obviously simplify the general equation given above. Also, in order to simplify the notation, the indices $\mu = \nu = 0$ shall not be explicitly written in the following discussion of results for hard ellipsoids.

In general, the calculation of the $A^{mnl\mu\nu}_{m'n'l'\mu'\nu'}(r)$ coefficients would involve five-dimensional numerical integrations over the angular variables. However, for axially symmetric particles the angular integration is reduced to three dimensions. Also one has the symmetry relationship

$$A^{mnl}_{m'n'l'}(r) = A^{nml}_{n'm'l'}(r) , \tag{28}$$

which obviously reduces the number of necessary calculations. It should be emphasized that the calculation of the $A^{mnl}_{m'n'l'}(r)$ coefficients is not part of the interation scheme used to solve the integral equations and must be performed only *once* for each value of a/b. Nevertheless, for relatively large basis sets the calculation of these functions is a major part of the computational effort and it is in fact the number of $A^{mnl}_{m'n'l'}(r)$ coefficients which eventually limits the number of terms it is practical to include in the correlation function expansions (see Table I). An outline of the numerical method used to calculate the $A^{mnl}_{m'n'l'}(r)$ coefficients for hard ellipsoids is given in Appendix B.

The results obtained for a given closure will depend to some extent upon the number of terms included in the rotational invariant expansion of the correlation functions. Therefore, in order to investigate the basis set dependence we have carried out calculations for the different basis sets summarized in Table I. The different basis sets are defined by the maximum values of the indices m, n, and l (i.e., $m_{max} = n_{max}$ and l_{max}) used in the calculation. The number of independent terms [i.e., terms related by Eq. (27) are only counted once] in each basis set as well as the number of independent [i.e., terms related by Eq. (28) are only counted once] $A^{mnl}_{m'n'l'}(r)$ coefficients are also given in Table I. The number of $A^{mnl}_{m'n'l'}(r)$ coefficients obviously grows rapidly with the number of terms in the expansion (cf. Table I, footnote b) and as mentioned above this eventually limits the number of terms which can be included in the calculation.

TABLE II. The basis set dependence of the HNC results for $a/b = 3$ and $\rho^* = 0.24$. The basis sets are defined in Table I.

Property	Basis Set I	Basis Set II	Basis Set III
$[\beta P(V)]/\rho$	13.6	13.1	13.8
$[\beta P(C)]/\rho$	8.15	8.12	...
χ_T/χ_T^0	0.0413	0.0416	0.0418
$\beta A K^{-1}$	0.485	0.478	0.506

The basis set dependence in the HNC results for hard ellipsoids with $a/b = 3$ and $\rho^* = 0.24$ is shown in Table II. The quantities $[\beta P(V)]/\rho$ and $[\beta P(C)]/\rho$ are the virial and

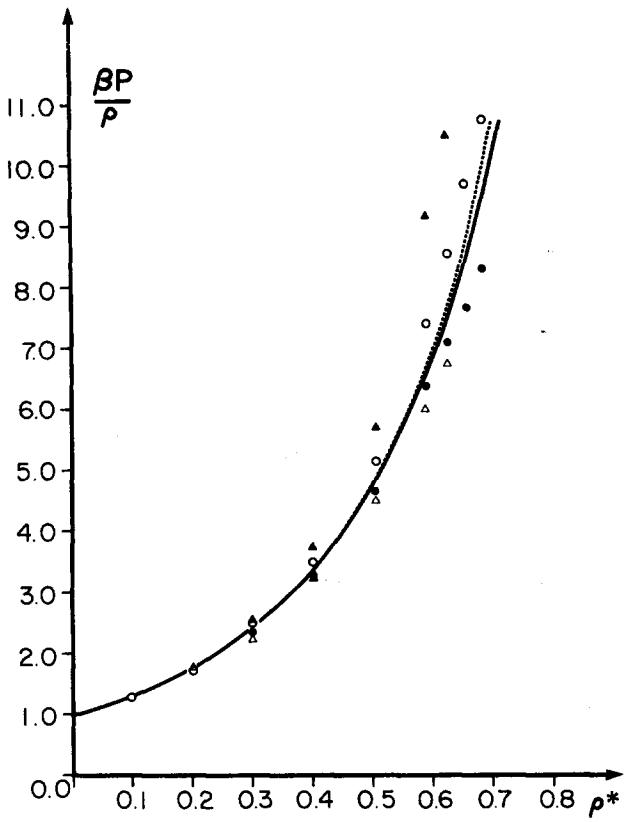

FIG. 1. The compressibility factor $\beta P/\rho$ for $a/b = 1.25$ obtained with basis set II. The solid curve represents the Monte Carlo data (Ref. 9) and the dashed curve is the y expansion (Ref. 9). The solid and open triangles are the HNC results obtained for the virial and compressibility equations, respectively. The solid and open circles are the PY results obtained from the virial and compressibility equations, respectively.

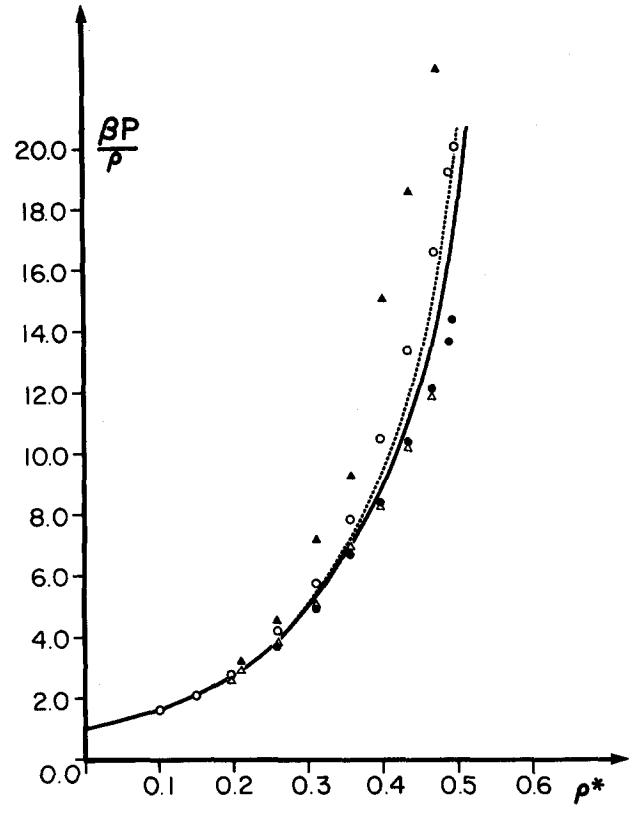

FIG. 2. The compressibility factor $\beta P/\rho$ for $a/b = 2$ obtained with basis set II. The curves are as in Fig. 1.

compressibility values as determined by Eqs. (20) and (26), respectively. The ratio of the isothermal compressibility to the ideal gas value χ_T/χ_T^0 is given by Eq. (23), and βAK^{-1} is a reduced reciprocal Kerr constant. The Kerr constant is important in analysis of the stability of the isotropic phase and is defined below [cf. Eq. (34)]. It can be seen from Table II that some basis set dependence is observed for $[\beta P(V)]/\rho$ but that $[\beta P(C)]/\rho$ and χ_T/χ_T^0 show very little variation. This is what we would expect since $[\beta P(C)]/\rho$ and χ_T depend *explicitly* only upon $g^{000}(r)$, whereas $[\beta P(V)]/\rho$ has an explicit dependence upon all the $g^{mnl}(r)$ projections [cf. Eq. (21)]. The Kerr constant explicitly depends upon $h^{220}(r)$ [cf. Eq. (34a)] and thus has a weak dependence upon basis set.

For the quantities given in Table II the basis set dependence in the PY results is either similar to or smaller than that found for the HNC theory. We note that the basis set dependence decreases with the a/b value and also with density. Therefore, the basis set dependence shown in Table II illustrates essentially the maximum observed for fluids compared with Monte Carlo calculations. We have investigated the basis set dependence only for $a/b = 3$, and the $a/b = 5$ results obtained with basis set II are included simply to given an idea of how very long ellipsoids are likely to behave. We certainly do not claim that the bais set II results are full HNC or PY solutions for this system. Finally, we note that

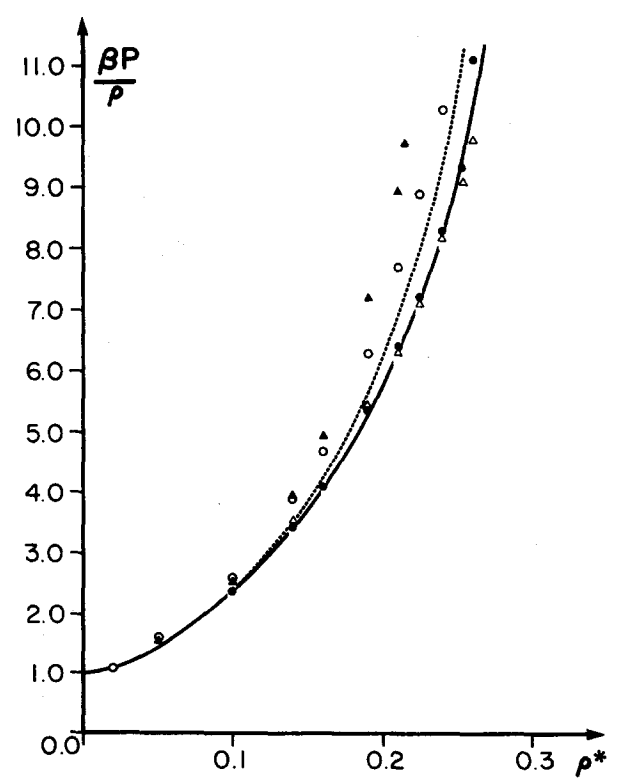

FIG. 3. The compressibility factor $\beta P/\rho$ for $a/b = 3$ obtained with basis set II. The curves are as in Fig. 1.

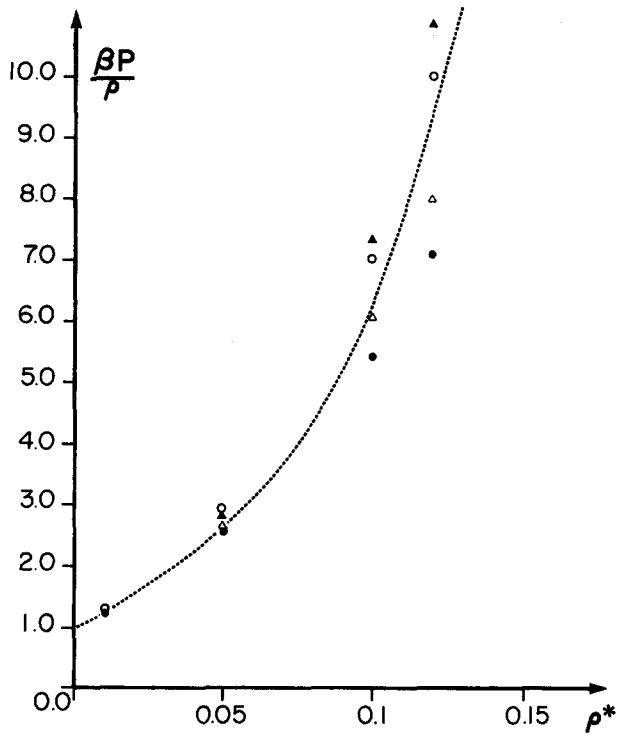

FIG. 4. The compressibility factor $\beta P/\rho$ for $a/b = 5$ obtained with basis set II. The curves are as in Fig. 1 except that there are no Monte Carlo results in this case.

the basis set dependence of $g^{000}(r)$ and $h^{220}(r)$ is discussed below (cf. Sec. III B).

A. The equation of state

The compressibility factor $\beta P/\rho$ for $a/b = 1.25$, 2, 3, and 5 is plotted in Figs. 1–4, respectively. All integral equation results shown in Figs. 1–4 were obtained with basis set II. We also included in the figures the theoretical equation of state given by the so-called y expansion applied to ellipsoids by Frenkel and Mulder.[9] For $a/b = 1.25$, 2, and 3 the theoretical results are compared with exact Monte Carlo values.[9] The y expansion is quite accurate for hard spheres[18] and is generally in better agreement with exact results than PY or HNC theories. For ellipsoids we find that this is also true for $a/b = 1.25$ and 2. However, for $a/b = 3$ more accurate equations of state are given by both the PY and HNC theories.

The curves shown in Fig. 1 for $a/b = 1.25$ resemble to some extent those for hard spheres with the PY results being more accurate than the corresponding HNC values. However, we observe that the PY(V) is slightly more accurate than the PY(C) (i.e., V and C denote the viral and compressibility results, respectively) whereas the opposite is true for hard spheres.[12,19] From Figs. 2 and 3 it can be seen that for $a/b = 2$ and 3 the PY(V) and HNC(C) results are very similar and are more accurate than the PY(C) and HNC(V) values. This is particularly true at $a/b = 3$ (cf. Fig. 3) where, as mentioned above, the PY(V) and HNC(C) are considerably more accurate than the y expansion. There are no exact Monte Carlo results for $a/b = 5$ but if the pattern observed in Fig. 3 holds then the PY(V) and HNC(C) are likely the most accurate theoretical results in this case as well.

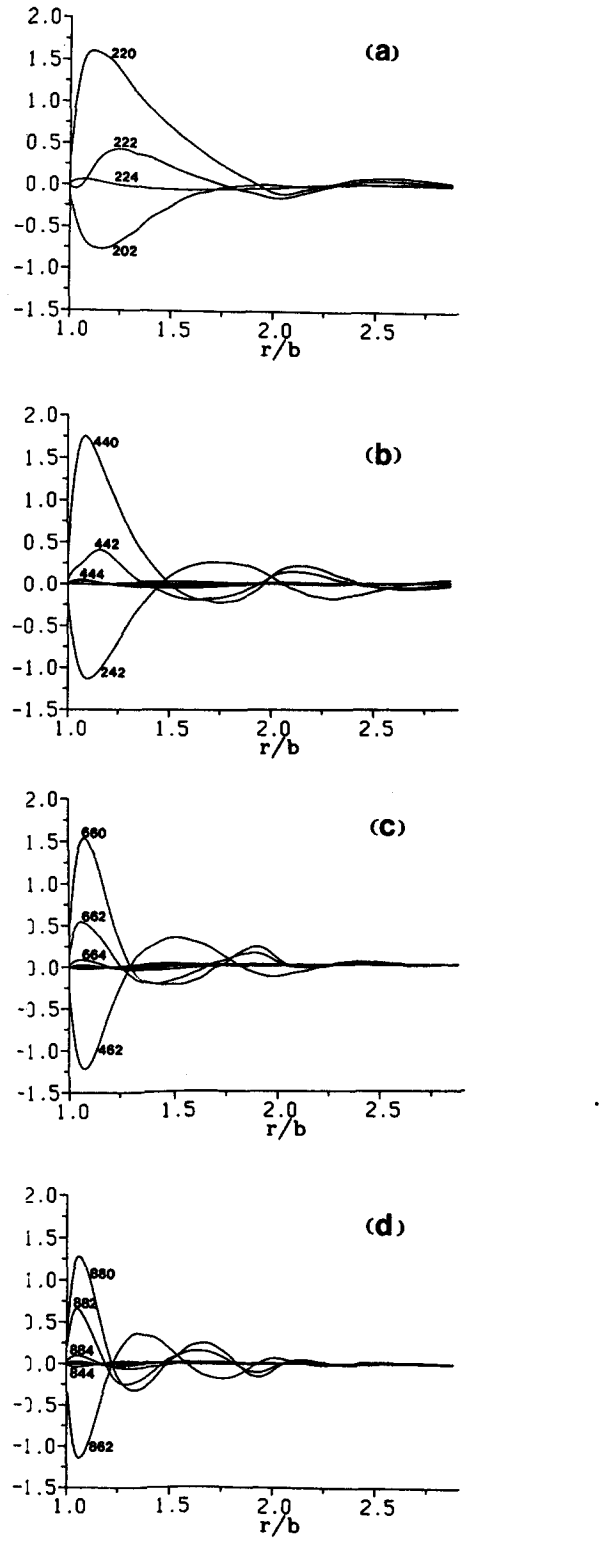

FIG. 5. The HNC results for $h^{mnl}(r)$ obtained with basis set III for $a/b = 3$ and $\rho^* = 0.24$. The four plots are as follows: (a) $(m,n) \leq 2$; (b) $(m,n) \leq 4$; (c) $(m,n) \leq 6$; (d) $(m,n) \leq 8$. Only those curves clearly discernable on the scale used in the figure are labeled with the appropriate (mnl) values.

B. The pair distribution function

From Eqs. (6) it is obvious that the magnitude of the $h^{mnl}(r)$ coefficients will depend upon the choice one makes

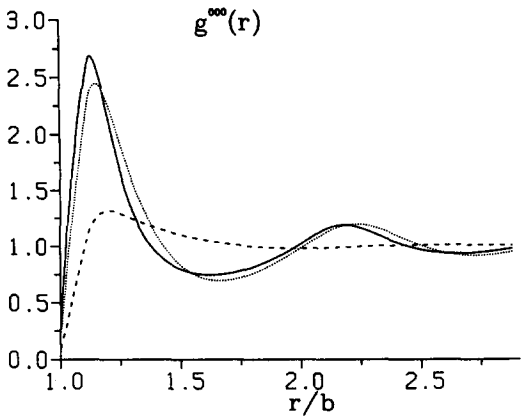

FIG. 6. The radial distribution function $g^{000}(r)$ for $a/b = 1.25$ obtained with basis set II. The solid and dotted curves are, respectively, HNC and PY results at $\rho^* = 0.624$. The dashed curve is at $\rho^* = 0.20$ where the HNC and PY results are not distinguishable on the scale used in the figure.

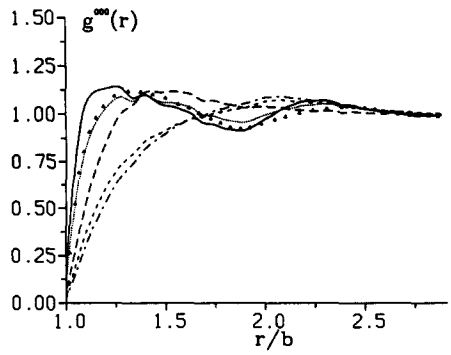

FIG. 8. The radial distribution function $g^{000}(r)$ for $a/b = 3$ obtained with basis set II. The solid, dotted, and short-dash curves are HNC results for $\rho^* = 0.26$, 0.24, and 0.14, respectively. The long-dash and dash–dot curves are PY results for $\rho^* = 0.24$ and 0.14, respectively. The solid triangles are Monte Carlo points (Ref. 10) for $\rho^* = 0.2546$.

for f^{mnl}. As in our earlier work[1–5] all functions shown in this paper are for the choice

$$f^{mnl} = l! \Big/ \begin{pmatrix} m & n & l \\ 0 & 0 & 0 \end{pmatrix}. \tag{29}$$

The $h^{mnl}(r)$ coefficients obtained with basis set III for $a/b = 3$ are shown in Fig. 5. It can be seen from the figures that the most important coefficients are those for which $l = 0$. For $l \neq 0$ the magnitude and importance of the projections fall very rapidly with increasing l regardless of the values of m and n. All coefficients with $l = 4$ are small and those for which $l = 6$ cannot be seen on the scale used in Fig. 5. Hence, no projections for which $l > 6$ are included in the basis sets.

The HNC results for $g^{000}(r)$ obtained with basis set II for $a/b = 1.25$, 2, 3, and 5 are shown in Figs. 6–9, respectively. At $a/b = 1.25$ (Fig. 6) one obtains a smooth curve with well-defined structural features. Indeed, $g^{000}(r)$ looks very similar to the radial distribution functions obtained for typical "soft" sphere fluids. At $a/b = 2$ and 3 (Figs. 7 and 8, respectively) the radial distribution functions have rather broad peaks with some "fine structure" at high density. The fine structure is not a numerical artifact [cf. note that the structure factors (Figs. 11 and 12) are smooth functions] but it does exhibit some dependence upon basis set (cf. Fig. 10). At $a/b = 3$ (Fig. 8) and particularly at $a/b = 5$ (Fig. 9) the HNC curves show a distinct peak developing at short range as the density is increased. This likely indicates an increasing tendency for the ellipsoids to form parallel configurations. This effect is also apparent in the $h^{220}(r)$ projections (cf. Figs. 14 and 15).

The PY results for $g^{000}(r)$ are also shown in Figs. 6–9. At low density the PY and HNC curves are very similar for all values of a/b. However, for relatively large values of a/b and high densities (cf. Figs. 7–9) significant discrepancies occur. Of particular importance is the fact that the PY approximation does not show the peak at short range evident in the HNC curves for $a/b = 3$ and $a/b = 5$. Again, this is consistent with the $h^{220}(r)$ results and is due to the fact that the PY approximation does not predict a strong preference for parallel configurations.

The basis set dependence of the HNC $g^{000}(r)$ for $a/b = 3$ and $\rho^* = 0.24$ is shown in Fig. 10. We note that basis sets II and III give very similar results but that the fine details do vary to some extent particularly at short range. All basis set dependence rapidly vanishes as the density is decreased. For $a/b = 3$ the PY result for $g^{000}(r)$ exhibits virtually no basis set dependence even at high density. In all cases we have looked at, basis sets I and II give essentially identical results.

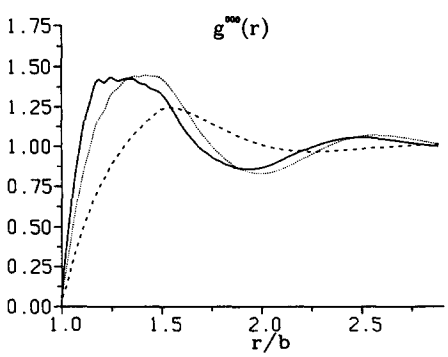

FIG. 7. The radial distribution function $g^{000}(r)$ for $a/b = 2$ obtained with basis set II. The solid and dotted curves are, respectively, the HNC and PY results at $\rho^* = 0.397$. The dashed curve is at $\rho^* = 0.20$ where the HNC and PY results are not distinguishable on the scale used in the figure.

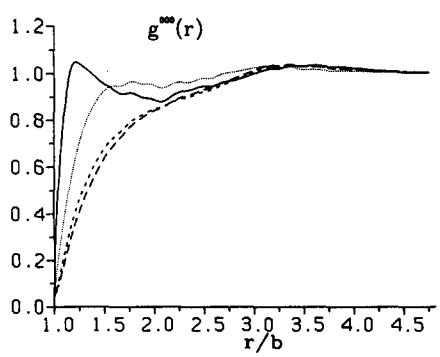

FIG. 9. The radial distribution function $g^{000}(r)$ for $a/b = 5$ obtained with basis set II. The solid and short-dash curves are HNC results for $\rho^* = 0.12$ and 0.05, respectively. The dotted and long-dash curves are PY results for $\rho^* = 0.12$ and 0.05, respectively.

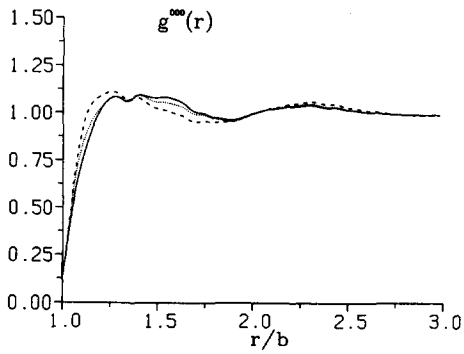

FIG. 10. The basis set dependence in the HNC result for $g^{000}(r)$ for $a/b = 3$ at $\rho^* = 0.24$. The solid dotted and dashed curves are for basis sets III, II, and I, respectively.

The Monte Carlo results for $g^{000}(r)$ with $a/b = 3$ reported by Perram *et al.*[10] are also shown in Fig. 8. We note that the overall shape of the Monte Carlo curve is similar to the integral equation results. The Monte Carlo points plotted in Fig. 8 were estimated from the *smooth* curve given in Ref. 10. Very precise Monte Carlo calculations would be necessary in order to test the fine detail in the theoretical results.

The structure factors defined by

$$S(k) = 1 + \rho \tilde{h}^{000}(k) \tag{30}$$

given by the HNC and PY theories for $a/b = 2$ and 3 are illustrated in Figs. 11 and 12, respectively. We note that these functions are basically unremarkable smooth curves. As we would expect from the $g^{000}(r)$ results the structural features in $S(k)$ become less distinct as a/b is increased.

The $h^{220}(r)$ projection is particularly important since its behavior determines the stability limit of the isotropic phase (cf. Sec. III C). HNC and PY results for $h^{220}(r)$ with $a/b = 2$, 3, and 5 are shown in Figs. 13–15, respectively. In order to obtain a physical understanding of this function it is useful to note that[5]

$$h^{220}(r) = \frac{5^{3/2}}{f^{220}} g^{000}(r) \langle P_2(\cos\beta) \rangle_r , \tag{31}$$

where β is the angle between the symmetry axes of the ellipsoids, $P_2(\cos\beta)$ represents the usual second order Legendre polynomial, and $\langle P_2(\cos\beta) \rangle_r$ denotes the average value *per particle* for a distance r. Thus for a given $g^{000}(r)$, $h^{220}(r)$ increases with increasing tendency towards parallel configurations. It can be seen from Figs. 13–15 that the HNC theory gives larger and sharper peaks at short range than those obtained with the PY approximation. Furthermore, for $a/b = 3$ and 5 (Figs. 14 and 15, respectively) and high density the HNC result for $h^{220}(r)$ is longer ranged than the PY function. A further discussion of the $h^{220}(r)$ projection and its importance in determining the stability limit of the isotropic phase is given below.

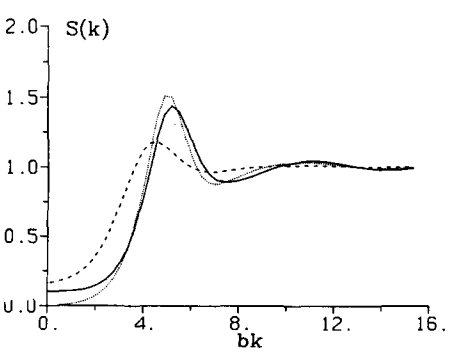

FIG. 11. The structure factor $S(k)$ for $a/b = 2$ obtained with basis set II. The solid and dotted curves are, respectively, the HNC and PY results at $\rho^* = 0.397$. The dashed curve is at $\rho^* = 0.20$ where the HNC and PY results are not distinguishable on the scale used in the figure.

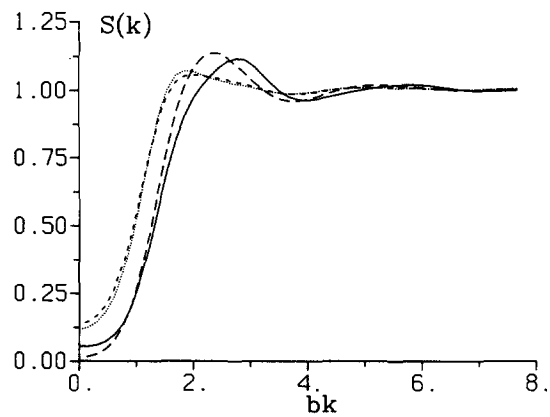

FIG. 12. The structure factor $S(k)$ for $a/b = 3$ obtained with basis set II. The solid and short-dash curves are HNC results for $\rho^* = 0.24$ and 0.14, respectively. The long-dash and dotted curves are PY results for $\rho^* = 0.24$ and 0.14, respectively.

The basis set dependence of the HNC result for $h^{220}(r)$ at $a/b = 3$ and $\rho^* = 0.24$ is shown in Fig. 16. It is apparent from the figure that although all three basis sets give similar functions, the height of the first peak does exhibit some dependence upon basis set. This is mainly due to the fact that projections of the type $h^{mm0}(r)$ do not decrease rapidly in magnitude with increasing m. Again the PY solutions show very little basis set dependence with basis sets I and II giving near identical results.

C. Stability of the isotropic phase

The condition for the stability of the isotropic phase relative to the nematic state can be expressed in the general form[5,11]

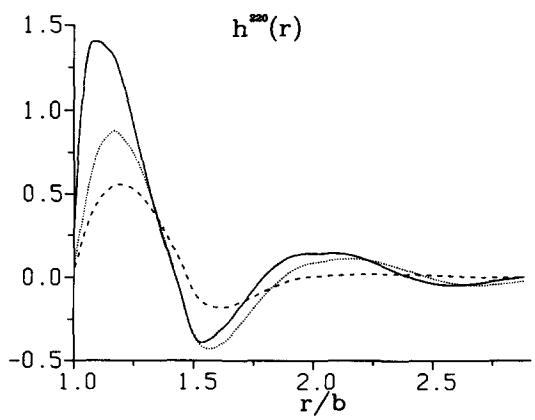

FIG. 13. The function $h^{220}(r)$ for $a/b = 2$ obtained with basis set II. The curves are as in Fig. 7.

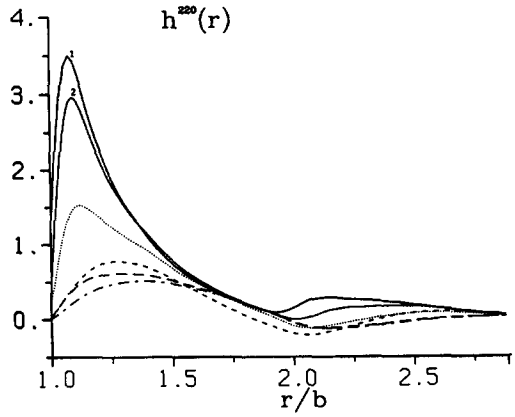

FIG. 14. The function $h^{220}(r)$ for $a/b = 3$ obtained with basis set II. The solid-1, solid-2, dotted, and long-dash curves are HNC results for $\rho^* = 0.27$, 0.26, 0.24, and 0.14, respectively. The short-dash and dash–dot curves are PY results for $\rho^* = 0.24$ and 0.14, respectively.

$$\left[1 - \frac{f^{mm0}}{(2m+1)^{3/2}} \rho \tilde{c}^{mm0}(0)\right] > 0, \tag{32}$$

where $m \neq 0$. It is important to emphasize that Eq. (32) determines the spinodal line and not the thermodynamic coexistance curve for the isotropic and nematic phases. This means that Eq. (32) does not give the thermodynamic isotropic–nematic transition density, but it does establish the limit beyond which the isotropic phase cannot exist even as a thermodynamically metastable state.

In Appendix A it is shown that for molecules of axial symmetry one has the exact relationship

$$\tilde{h}^{mm0}(0) = \frac{\tilde{c}^{mm0}(0)}{1 - [f^{mm0}/(2m+1)^{3/2}]\rho\, \tilde{c}^{mm0}(0)}. \tag{33}$$

It is interesting to note that this equation which we obtained previously for specific $P_2(\cos\beta)$ potentials[5] is in fact valid for all axially symmetric models. A more general result for particles of arbitrary symmetry is obtained in Appendix A. Equation (33) allows us to easily understand the physical significance of Eq. (32). It is obvious that, as the denominator on the left hand side of Eq. (32) tends to zero, $\tilde{h}^{mm0}(0) \to \infty$. Hence Eq. (32) simply expresses the fact that

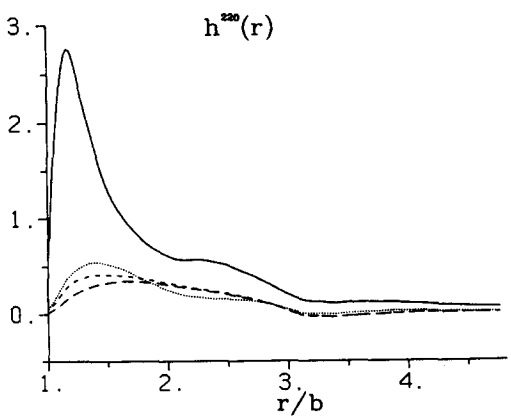

FIG. 15. The function $h^{220}(r)$ for $a/b = 5$ obtained with basis set II. The curves are as in Fig. 9.

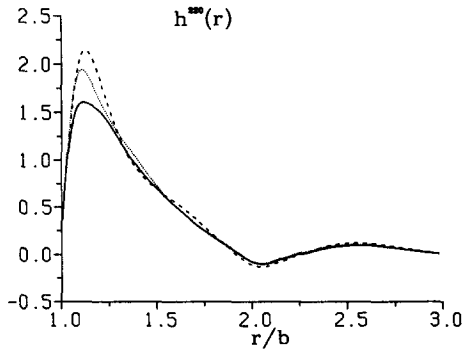

FIG. 16. The basis set dependence in $h^{220}(r)$ for $a/b = 3$ and $\rho^* = 0.24$. The curves are as in Fig. 10.

the isotropic phase must become unstable as the angular correlations become of infinite range. In practice, we find both for simple $P_2(\cos\beta)$ models[5] and in the present calculations for ellipsoids, that the stability limit of the isotropic phase is determined by the divergence of $\tilde{h}^{220}(0)$.

Experimentally, this phenomena is observed in measurements of the static Kerr constant.[20,21] For axially symmetric nondipolar particles such as the present model the Kerr constant is defined by[22]

$$K = \beta A \left[1 + \frac{f^{220}}{5^{3/2}} \tilde{h}^{220}(0)\right] \tag{34a}$$

$$= \beta A \left[1 - \frac{f^{220}}{5^{3/2}} \tilde{c}^{220}(0)\right]^{-1}, \tag{34b}$$

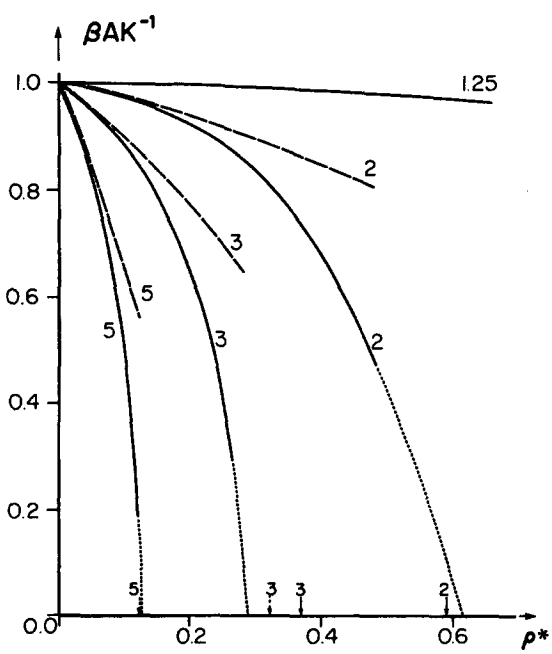

FIG. 17. The reduced inverse Kerr constant $\beta A K^{-1}$ as a function of density. The values of a/b for the different curves are given on the plot. The calculated and extrapolated HNC curves are represented by solid and dotted lines, respectively. The dashed curves denote the calculated PY results. The solid arrows indicate the Monte Carlo liquid→solid transition densities (Ref. 9). The Monte Carlo isotropic→nematic transition density (Ref. 9) for $a/b = 3$ is indicated with dashed arrow. A dashed arrow also marks the isotropic→nematic transition predicted by the y expansion (Ref. 9) for $a/b = 5$.

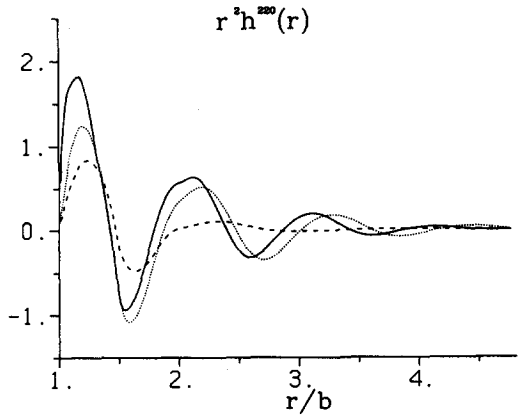

FIG. 18. The function $r^2h^{220}(r)$ for $a/b = 2$ obtained with basis set II. The curves are as in Fig. 7.

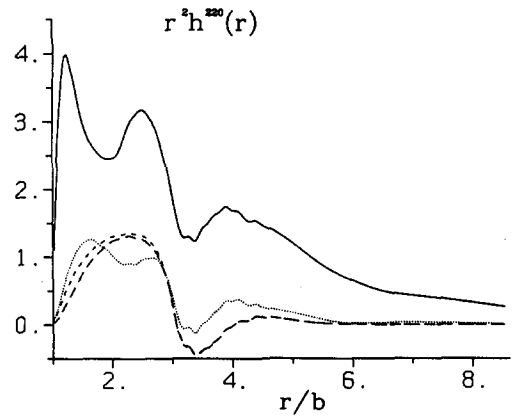

FIG. 20. The function $r^2h^{220}(r)$ for $a/b = 5$ obtained with basis set II. The curves are as in Fig. 9.

where A depends upon molecular parameters,[5] and Eq. (34b) is obtained with the aid of Eq. (33). It is clear from this definition that K must diverge and $K^{-1} \to 0$ as the isotropic phase becomes unstable.

In Fig. 17 the quantity βAK^{-1} is plotted as a function of ρ^*. For $a/b = 2$ and 3 the density of the liquid→solid transition as reported by Frenkel and Mulder[9] is marked with solid arrows. The Monte Carlo result[9] for the isotropic–nematic transition density at $a/b = 3$ is indicated by a broken arrow. As noted above, Monte Carlo results are not available for $a/b = 5$, but the isotropic–nematic transition density predicted[9] by the y expansion is also marked with a broken arrow. It is obvious from Fig. 17 that, as we would expect, the rate at which βAK^{-1} approaches zero increases rapidly with increasing values of a/b. It is also apparent that the PY curves fall more slowly than the corresponding HNC results. For $a/b = 2$ both the extrapolated HNC and PY curves fail to reach zero before the liquid→solid transition density. Hence the theoretical results strongly suggest that the isotropic phase is stable throughout the liquid regime and this is in fact consistent with the Monte Carlo calculations. At $a/b = 3$ the extrapolated HNC curve does cross zero before the freezing density. Thus the HNC theory does predict the existence of a nematic phase. Furthermore, the value of ρ^* at which $\beta AK^{-1} = 0$ is close to the density of the isotropic–nematic transition given by Frenkel and Mulder.[9] The extrapolated PY result, on the other hand, does not reach zero before the freezing transition and thus in the PY approximation the isotropic phase remains stable. At $a/b = 5$ the HNC result for $\tilde{h}^{220}(0)$ also diverges and βAK^{-1} falls rapidly to zero, predicting a nematic phase at very low density in good agreement with the y expansion.

In order to obtain a physical picture of what is happening in these fluids as the isotropic phase becomes unstable, we have plotted $r^2h^{220}(r)$ for $a/b = 2$, 3, and 5 in Figs. 18–20, respectively. This is clearly the correct function to plot since its integral with respect to r determines $\tilde{h}^{220}(0)$. We note that for $a/b = 2$ both the HNC and PY functions oscillate about zero and rapidly decay. At $a/b = 3$ and 5 the PY curves continue to behave in a similar manner. However, the HNC result at higher densities changes quite dramatically and one can clearly see the development of a long-range correlation. This correlation is associated with the tendency to form parallel configurations and it is the growth of this correlation with density which eventually leads to the divergence of $\tilde{h}^{220}(0)$ and to the instabilty of the isotropic phase. Another illustration of this is given in Fig. 21 where we have plotted $\tilde{h}^{220}(k)$ for $a/b = 3$. The rapid increase in the small k values as ρ^* is increased is evident in the figure. Similar plots of the PY results do not exhibit this behavior.

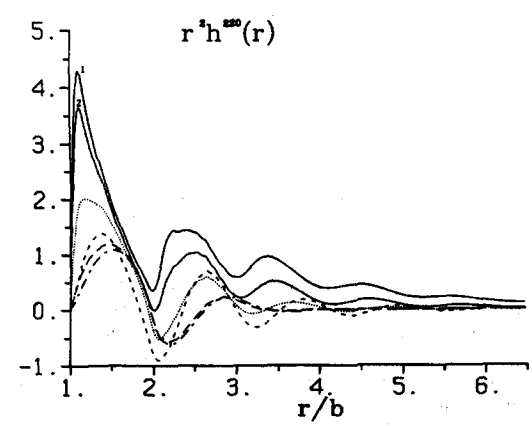

FIG. 19. The function $r^2h^{220}(r)$ for $a/b = 3$ obtained with basis set II. The curves are as in Fig. 14.

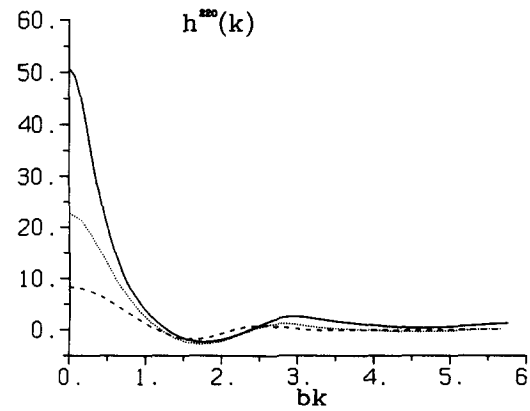

FIG. 21. HNC results for the Fourier transform $\tilde{h}^{220}(k)$ for $a/b = 3$ obtained with basis set II. The solid, dotted, and dashed curves are for $\rho^* = 0.27$, 0.24, and 0.14, respectively.

IV. CONCLUSIONS

In this paper it is shown how the HNC and PY integral equation theories can be solved for fluids of *hard* nonspherical particles. Such models differ significantly from those considered in our earlier calculations[1–5] in that they are defined by pair potentials which are discontinuous in orientational space. The formulation described in the present article takes proper account of this discontinuous behavior.

Numerical solutions of the HNC and PY theories have been obtained for systems of hard ellipsoids of revolution. Different models characterized by length-to-breadth ratios of $a/b = 1.25$, 2, 3, and 5 have been considered and results are reported for a wide range of densities. Wherever possible comparisons are made with previous Monte Carlo calculations.[9,10] It is found that in general the PY virial and HNC compressibility equations give very similar and reasonably accurate results for the equation of state. This differs from the hard sphere case where the PY compressibility route provides the most accurate values at high density. We also note that the PY(V) and HNC(C) results are more accurate than the y expansion[9] at $a/b = 3$.

Unfortunately, the Monte Carlo studies of ellipsoids have provided very little information about the pair distribution function, $g(r,\Omega_1,\Omega_2)$. For $a/b = 3$ we do compare the HNC and PY results for the radial distribution function, $g^{000}(r)$, with the Monte Carlo curve reported by Perram *et al.*[10] This serves to show that the HNC, PY, and Monte Carlo curves are all at least roughly similar in shape.

We have also investigated the orientational stability of the isotropic phase for ellipsoids of varying dimension. This is done by calculating the static Kerr constant which in the language of the present paper is related to $\tilde{h}^{220}(k=0)$ [cf. Eq. (34a)]. As the isotropic phase becomes unstable $h^{220}(r)$ becomes long-ranged such that both $\tilde{h}^{220}(0)$ and the Kerr constant diverge. Physically, this is due to the growth of long-ranged angular correlations favoring parallel orientations. It is found that for $a/b = 3$ the HNC theory predicts that the isotropic phase becomes unstable at a density which is considerably lower than the Monte Carlo freezing transition. Furthermore, the density at which the instability occurs is quite close to the density of the isotropic–nematic transition observed in the computer simulations.[9] The HNC results also indicate an orientational instability at rather low density for the $a/b = 5$ case in accord with the prediction of the y expansion.

The PY approximation, on the other hand, does not exhibit the rapid growth in the long-ranged orientational correlations evident in the HNC results. Thus for $a/b = 3$ the PY calculations do not predict a nematic phase. This also seems to be true for $a/b = 5$. Thus it appears that, at least for fluids of hard ellipsoids, the PY theory is not capable of producing the long-ranged orientational correlations which lead to isotropic–nematic phase transitions. This is perhaps not very surprising since we cannot expect the PY closure, which simply sets $c(12) = 0$ for all nonoverlapping configurations, to give an accurate account for long-range correlations.

In summary, we conclude that the HNC theory gives a reasonably good description of fluids of hard ellipsoids. It predicts a nematic phase and should be particularly useful for studying phenomena related to the growth of long-ranged angular correlations in the pretransitional region. The PY theory is less interesting for the reasons given above. Further, investigations of these theories for other fluids of hard nonspherical particles are being carried out and the integral equation techniques are being extended into the nematic regime.

ACKNOWLEDGMENTS

Acknowledgment is made to the Donors of the Petroleum Research Fund, administered by the American Chemical Society, for partial support of this research. We are also grateful for the financial support of the Natural Sciences and Engineering Research Council of Canada.

APPENDIX A: THE OZ EQUATION AT $k=0$. DERIVATION OF EQS. (24) AND (33)

In manipulations of the OZ equation it is sometimes convenient to choose

$$f^{mnl} = \sqrt{(2m+1)(2n+1)} \tag{A1}$$

in Eq. (6d). In the χ-transform language of Blum[13] the OZ relationships can then be expressed in the form

$$\tilde{N}^{mn}_{\mu\nu,\chi}(k) = \rho \sum_{n_1} \sum_{\nu_1=-n_1}^{n_1} (-)^{\chi+\nu_1} \times [\tilde{N}^{mn_1}_{\mu\nu_1,\chi}(k) + \tilde{C}^{mn_1}_{\mu\nu_1,\chi}(k)]\tilde{C}^{n_1 n}_{-\nu_1\nu,\chi}(k) , \tag{A2a}$$

where

$$\tilde{C}^{mn}_{\mu\nu,\chi}(k) = \sum_{l=|m-n|}^{m+n} \begin{pmatrix} m & n & l \\ \chi & -\chi & 0 \end{pmatrix} \tilde{c}^{mnl}_{\mu\nu}(k) , \tag{A2b}$$

$$\tilde{N}^{mn}_{\mu\nu,\chi}(k) = \sum_{l=|m-n|}^{m+n} \begin{pmatrix} m & n & l \\ \chi & -\chi & 0 \end{pmatrix} \tilde{\eta}^{mnl}_{\mu\nu}(k) . \tag{A2c}$$

Now for hard particles it is clear from Eq. (8b) that at $k = 0$ the only nonzero Hankel transforms are those with $l = 0$. Therefore, Eq. (A2b) immediately reduces to

$$\tilde{C}^{mn}_{\mu\nu,\chi}(0) = \begin{pmatrix} m & n & 0 \\ \chi & -\chi & 0 \end{pmatrix} \tilde{c}^{mn0}_{\mu\nu}(0) \tag{A3a}$$

$$= 0 \quad \text{if } m \neq n , \tag{A3b}$$

where Eq. (A3b) follows from the properties of the 3-j symbols (i.e., m, n, and l must satisfy the triangular inequalities). Of course equations analogous to (A3a) and (A3b) also connect $\tilde{N}^{mnl}_{\mu\nu,\chi}(0)$ and $\tilde{\eta}^{mnl}_{\mu\nu,\chi}(0)$. These relationships together with the formula[15]

$$\begin{pmatrix} m & m & 0 \\ \chi & -\chi & 0 \end{pmatrix} = \frac{(-)^{m-\chi}}{\sqrt{2m+1}} \tag{A4}$$

allow Eq. (A2a) (at $k = 0$) to be rewritten in the form

$$\tilde{\eta}^{mn0}_{\mu\nu}(0) = \frac{(-)^m}{\sqrt{2m+1}} \sum_{\nu_1=-m}^{m} (-)^{\nu_1} \times [\tilde{\eta}^{mm0}_{\mu\nu_1}(0) + \tilde{c}^{mm0}_{\mu\nu_1}(0)]\tilde{c}^{mm0}_{-\nu_1\nu}(0) . \tag{A5}$$

If we now consider the case $\mu = \nu = 0$ Eq. (A5) gives

$$\tilde{\eta}^{000}_{00}(0) = \rho[\tilde{\eta}^{000}_{00}(0) + \tilde{c}^{000}_{00}(0)]\tilde{c}^{000}_{00}(0) , \tag{A6}$$

which is exactly analogous to the OZ equation at $k=0$ for systems of spherical particles. Using the definition

$$\eta(12) = h(12) - c(12)\,, \tag{A7}$$

Eq. (A6) can be immediately rearranged to obtain Eq. (24).

In order to consider the stability condition defined by Eq. (32) and to derive Eq. (33) we must consider the case $\mu=\nu=0$ and m is even. Then using Eqs. (A5) and (A7) and reintroducing f^{mm0} as an *unspecified* constant it is easy to obtain the relationship:

$$\tilde{h}_{00}^{mm0}(0) - \tilde{c}_{00}^{mm0}(0) = \frac{f^{mm0}}{(2m+1)^{3/2}}\rho \sum_{\nu_1=-m}^{m} \tilde{h}_{0\nu_1}^{mm0}(0)\tilde{c}_{-\nu_1 0}^{mm0}(0)\,, \tag{A8a}$$

which can be rearranged to give

$$\tilde{h}_{00}^{mm0}(0) = \frac{\tilde{c}_{00}^{mm0}(0) + Y}{\{1 - [f^{mm0}/(2m+1)^{3/2}]\rho\,\tilde{c}_{00}^{mm0}(0)\}}\,, \tag{A8b}$$

where Y is just the sum on the right-hand side of Eq. (A8a) with the $\nu_1=0$ term excluded. From Eqs. (32) and (A8b) it follows that for molecules of any symmetry $\tilde{h}^{mm0}(0)$ will diverge as the isotropic phase becomes unstable. Also for axially symmetric molecules where only projections of the type $h_{00}^{mnl}(r)$ are allowed it is obvious that $Y=0$ and Eq. (A8b) becomes Eq. (33).

APPENDIX B: THE NUMERICAL CALCULATIONS OF THE $A_{m'n'l'}^{mnl}(r)$ FOR HARD ELLIPSOIDS OF REVOLUTION

For ellipsoids of revolution, Eq. (12b) can be written in the form

$$I^{mnl}A_{m'n'l'}^{mnl}(r) = \int_{ov} d\phi \sin\theta_1\, d\theta_1 \sin\theta_2\, d\theta_2 \times \Phi^{mnl}(12)\Phi^{m'n'l'}(12)\,, \tag{B1}$$

where

$$\cos\theta_1 = \hat{\mathbf{u}}_1\cdot\hat{\mathbf{r}}, \tag{B2}$$

$$\cos\theta_2 = \hat{\mathbf{u}}_2\cdot\hat{\mathbf{r}}\,, \tag{B3}$$

$$\cos\phi = (\hat{\mathbf{u}}_1\times\hat{\mathbf{r}})\cdot(\hat{\mathbf{u}}_2\times\hat{\mathbf{r}})\,. \tag{B4}$$

In Eqs. (B2)–(B4) $\hat{\mathbf{r}} = \mathbf{r}/|\mathbf{r}|$, where $\mathbf{r}$ is the vector joining the centers of ellipsoids 1 and 2, and $\hat{\mathbf{u}}_i$ is a unit vector directed along the major axis of ellipsoid i. Equation (B1) can be rewritten in the form

$$I^{mnl}A_{m'n'l'}^{mnl}(r) = \int_0^{2\pi} d\phi \int_0^{\pi} \sin\theta_1\, d\theta_1 \times\left[\int_0^{\theta_a} \sin\theta_2\, d\theta_2\, \Phi^{mnl}(12)\Phi^{m'n'l'}(12) + \int_{\theta_b}^{\pi} \sin\theta_2\, d\theta_2\, \Phi^{mnl}(12)\Phi^{m'n'l'}(12)\right], \tag{B5}$$

where θ_a and θ_b are the angles determining the overlap region. For fixed values of ϕ and θ_1 one can verify that no overlaps occur if $\theta_a < \theta_2 < \theta_b$.

In order to evaluate the three-dimensional integral in Eq. (B5) numerically it is convenient to proceed as follows. First a grid of N points is choosen for each angular variable. Then for each grid point the contact distance $\sigma(\theta_1,\theta_2,\phi)$ is found by solving the equation

$$\Psi(\sigma,\theta_1,\theta_2,\phi) = 0\,, \tag{B6}$$

where Ψ is the contact function defined in Ref. 6. The σ values are tabulated for each grid point.

For the required values of r (i.e., $b<r<a$) the integrals over ϕ and θ_1 can be carried out using a convenient quadrature formula (Simpson's rule was used in the present work) on the grid points selected above. The limits θ_a and θ_b on the θ_2 integration are determined by the overlap condition

$$\sigma(\theta_1,\theta_2,\phi) > r\,. \tag{B7}$$

For fixed θ_1, ϕ, and r precise values of θ_a and θ_b are found by inverse interpolation on the contour $\sigma(\theta_1,\theta_2,\phi) = r$ using the results tabulated earlier. The θ_2 integrations can then be performed.

Obviously, the accuracy of this procedure will depend upon the number of grid points used. For ellipsoids, tests with known integrals (i.e., at $r=a$ and $r=b$) indicate that $N=41$ is sufficient to give values of $A_{m'n'l'}^{mnl}(r)$ which are accurate to at least four significant figures. This is comparable to the accuracy in numerical solutions of the integral equations.

[1] P. H. Fries and G. N. Patey, J. Chem. Phys. **82**, 429 (1985).
[2] P. H. Fries and G. N. Patey, J. Chem. Phys. **85**, 7307 (1986).
[3] L. Y. Lee, P. H. Fries, and G. N. Patey, Mol. Phys. **55**, 751 (1985).
[4] J. S. Perkyns, P. H. Fries, and G. N. Patey, Mol. Phys. **57**, 529 (1986).
[5] A. Perera, P. G. Kusalik, and G. N. Patey, Mol. Phys. **60**, 77 (1987).
[6] V. Baron, Mol. Phys. **28**, 809 (1974).
[7] J. W. Perram and M. S. Wertheim, J. Comp. Phys. **58**, 409 (1985).
[8] V. Baron, J. Chem. Phys. **56**, 4729 (1972).
[9] D. Frenkel and B. M. Mulder, Mol. Phys. **55** 1171, 1193 (1985).
[10] J. W. Perram, M. S. Wertheim, J. Lebowitz, and C. O. Williams, Chem. Phys. Lett. **105**, 277 (1984).
[11] J. Stecki and A. Kloczkowski, J. Phys. Paris, **40**, C3-360 (1979); Mol. Phys. **42**, 51 (1981).
[12] J. P. Hansen and I. R. McDonald, *Theory of Simple Liquids* (Academic, New York, 1976).
[13] L. Blum and A. J. Torruella, J. Chem. Phys. **56**, 303 (1972); L. Blum, *ibid.* **57**, 1862 (1972); **58**, 3295 (1973).
[14] H. L. Friedman, *A Course in Statistical Mechanics* (Prentice-Hall, Englewood Cliffs, 1985).
[15] A. Messiah, *Quantum Mechanics* (Wiley, New York, 1962), Vol. II.
[16] S. L. Carnie, D. Y. C. Chan, and G. R. Walker, Mol. Phys. **43**, 1115 (1981).
[17] J. M. Caillol, Chem. Phys. Lett. **121**, 347 (1985).
[18] B. Barboy and W. M. Gelbart, J. Chem. Phys. **71**, 3053 (1979).
[19] J. A. Barker and D. Henderson, Rev. Mod. Phys. **48**, 587 (1976).
[20] J. C. Filippini and Y. Poggi, J. Phys. Lett. **35**, 99 (1974).
[21] H. J. Coles and B. R. Jennings, Mol. Phys. **31**, 571 (1976).
[22] S. Kielich, *Dielectric and Related Molecular Processes* (Chemical Society of London, London, 1972), Vol. 1, Chap. 7.